Performing three dimensional measurements on micro-scale features using a flexible CMM fiber probe with ellipsoidal tip

B. Muralikrishnan, J. Stone, C. Shakarji, and J. Stoup
Semiconductor and Dimensional Metrology Division
National Institute of Standards and Technology
Gaithersburg MD 20899

Abstract: The tip of a traditional Coordinate Measuring Machine (CMM) probe used for measurements of macro-scale artifacts is generally a sphere of excellent geometry. Its known diameter (from a prior calibration) and form, along with the known approach direction (which is normal to the surface), facilitate probe radius compensation in a straightforward manner. Neither of these conditions is valid for micro-scale measurements made with a flexible fiber probe on a CMM. This presents two challenges. The first involves the calibration of the probe's true size and shape. The second involves developing a method for compensating probe radius and form on measurement data from test artifacts. We describe these issues here in the context of an application involving three-dimensional measurements on micro-scale features (a conical section of 20° half angle and a rounded tip of 38 μm radius) performed with the NIST fiber probe [1].

1. Introduction

Fiber probes are increasingly used for dimensional metrology of micro-scale features on CMMs. These delicate probes have slender stems (5 mm to 20 mm long, 10 μm to 100 μm in diameter) with a ball (50 μm to 200 μm diameter) at the end. Surface contact may be detected by different techniques; see [2, 3] for a review of micro probing techniques.

Unlike the probing spheres of a traditional CMM, the geometry of a fiber probe tip is difficult to control. Deviations from sphericity of several micrometers are possible on a ball of 100 μm diameter, especially if the ball is manufactured as an integral piece with the stem. In fact, integrally manufactured probes, particularly those made of glass, have a tear drop shape [4], the bottom half of which can be approximated more closely as a spheroid or an ellipsoid instead of a hemisphere, as measurements on precision spheres using our NIST fiber probe have shown. Such non-spherical form poses a measurement and data analysis challenge in terms of both calibrating the probe size/shape and also in compensating for probe size/shape from measured data on test artifacts.

There is also another measurement and data analysis challenge associated with fiber probe measurements. The flexible stems of fiber probes are free to oscillate in the presence of air currents and therefore the actual point of contact of the probe on the surface may not be the desired point of contact, see Fig. 1. Because part sizes are small and comparable to other dimensions such as probe size and amplitude of oscillation, the surface normal at the point of contact may be oriented in a significantly different direction than the approach direction. Therefore, even if the probe ball were spherical in form, probe radius compensation would involve determination of the direction of surface normals at the point of contact (note that the actual point of contact is a known quantity

while the surface normal is not). With non-spherical probes, the problem of probe size/shape compensation becomes a more challenging mathematical problem.

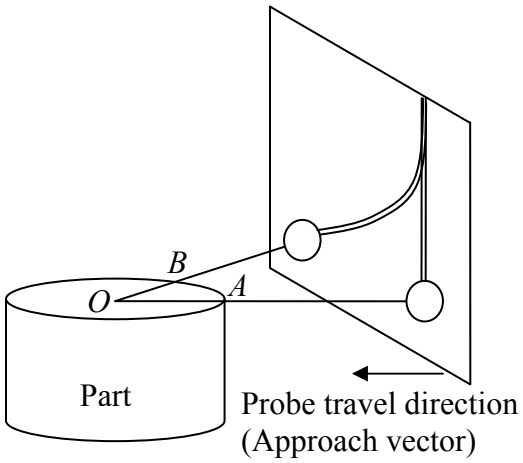

Fig. 1 Probe travel direction is along AO. The theoretical point of contact is at A, but the flexible fiber can oscillate due to machine vibrations or air currents and therefore the actual point of contact is at B. Because the part size is small and comparable to other dimensions such as probe size and amplitude of oscillation, the surface normal at B (OB) is significantly different from that at A (OA).

We describe these problems and our solution approach in the context of an application involving the measurement of a conical feature with a radiused tip, using our NIST fiber probe. The nominal half angle of the cone is 20° and the radius at the tip is about 38 μm. The region of interest is the top 130 μm portion of the part, see Fig. 2.

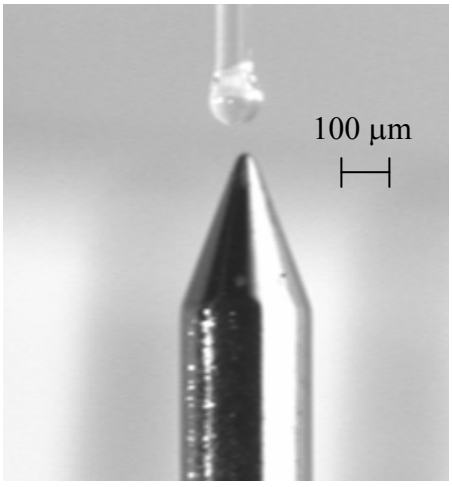

Fig. 2 A photo of the test artifact and the probe.

The principle of operation of the NIST fiber probe has been reported earlier [1] and we do not describe it here. The techniques we describe in this paper are not specific to the measurement technology; rather they pertain to all types of flexible micro-probes that may not have a high quality tip. We describe the calibration and validation of the probe tip parameters in Section 2, three dimensional measurement of micro-scale features on

the test artifact in Section 3, and summarize our observations and conclusions in Section 4.

At the outset, we point out that our approach of calibrating the shape of an ellipsoidal tip so that the form information may then be used in subsequent measurements, relies on the assumption that probe, although flexible, returns to its equilibrium state and that there is no change in the tilt of the probe during the period of the measurements. We believe such an assumption is reasonable; calibration measurements performed before and after measurement of a test artifact have provided identical values for probe tilt parameters suggesting negligible tilt in the probe over reasonably short periods of time (two to three days).

We also note that the probe is in fact placed within an enclosure, but that enclosure is not air tight because the ram of the machine must be free to move so that it can carry the probe to the different probing locations. A plastic drape does fall from the ram on to a shell around the part, but it not a rigid coupling. This is intentional because a rigid coupling between the ram and the table will produce small but sufficient forces that cause distortion in the measurement. Therefore, the effect of air currents cannot be completely eliminated.

2. Calibration and validation of probe ball parameters

2.1 Setup

The artifacts we used for calibrating and verifying the probe ball parameters are two steel master spheres of 3/16 in (4.7625 mm) and 5/16 in (7.9375 mm) nominal diameter. Their diameters have been measured using interferometry at NIST to be 4762.42 μm and 7937.88 μm with an expanded uncertainty of 10 nm (k = 2). With our fiber probe, we measured 16 data points per circular trace and 8 circular traces on these spheres at elevations of zero through 70º in intervals of 10º. We also measured the pole point on each sphere for a total of 129 data points per sphere.

As part of the set-up procedure, we first determine the position of the equatorial plane of the calibration sphere in machine coordinates by measuring circular traces at closely spaced Z positions. Subsequently, a circular trace at the equator provides an estimate of the equatorial radii a and b of the probe ball. We then probe the pole point to get an estimate of the polar radius c of the probe ball. These measurements indicated that the probe was probably spheroidal in shape with an equatorial radius of approximately 32 μm and a polar radius of approximately 36 μm.

Assuming therefore the probe is spheroidal in shape, we positioned the probe at the appropriate heights for the two spheres so that the point of contact occurs at the same position on the probe for all elevations. This is illustrated in Fig. 3. To measure coordinate A on the sphere at an elevation of θ, a spherical probe (as in Fig. 3(a)) has to be positioned at C which is at a height of $(R+r)\sin\theta$ where all relevant variables are defined in Fig. 3. If the probe is ellipsoidal and represented by the

equation $\frac{x^2}{a^2}+\frac{y^2}{b^2}+\frac{z^2}{c^2}=1$, its parametric form is given by $x = a\cos\eta\cos\phi$, $y = b\cos\eta\sin\phi$, $z = c\sin\eta$, where η and ϕ are the parameters of the ellipsoid. Then, the probe has to be positioned at *D* which is at a height of $R\sin\theta+c\sin\eta$. The requirement that the two surfaces in contact have the same normal vector gives $\eta = \tan^{-1}(c\sqrt{\frac{\cos^2\phi}{a^2}+\frac{\sin^2\phi}{b^2}}\tan\theta)$. For spheroidal probes, $a = b$, therefore $\eta = \tan^{-1}(\frac{c}{a}\tan\theta)$.

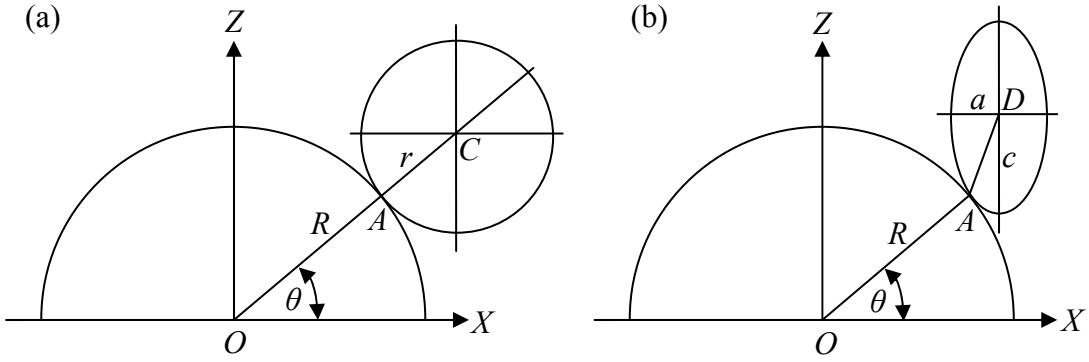

Fig. 3(a) Positioning a spherical probe along Z to measure coordinate A at an elevation of θ. (b) Positioning an ellipsoidal probe to measure the same coordinate A.

2.2 Sphere fit

Although we are aware that the probe ball is not spherical in shape, we present diameter and form results assuming the probe ball is indeed spherical to highlight the magnitude and nature of the errors in such an assumption.

The probe diameter is determined by measuring the probe ball against our calibration sphere. An unconstrained least-squares best fit sphere (we determine both sphere center and diameter through the fit) to the calibration data yields a probe diameter of 64.44 μm. The probe is then used to measure the diameter of a check sphere. A similar fit to determine the diameter of the check sphere yields a diameter of 7937.87 μm after correcting for probe size. This value is only 10 nm smaller than the calibrated value of the check sphere, which is 7937.88 μm. While the error in the diameter is small, the form error is large, see Fig. 4. The residuals are larger near the equator and the pole but smaller for other elevations near the middle, suggesting that the best-fit sphere has been translated along the *Z* direction, as might be expected when fitting a sphere to a spheroidal data set consisting of measurements on the upper hemisphere only. The *Z* center data in fact confirms this; the center appears to be translated along *Z* by about 3 μm for both spheres from the experimentally determined equatorial plane position. We should note that while the error in the diameter is only 10 nm on the 5/16 in (7.94 mm) check sphere [after calibrating the probe ball using the 3/16 in (4.76 mm) calibration

sphere], simulations reveal that the error is much larger, on the order of 100 nm, for smaller sized hemispheres such as those considered in Section 3.

We then constrained the *Z* positions to the experimentally known values and recalculated the least square sphere center and radius for the two spheres. The probe diameter obtained from the calibration sphere was 67.66 µm, which is more than 3 µm larger than that determined from an unconstrained fit. The diameter of the check sphere was 7937.83 µm, which is 0.05 µm smaller than the calibrated value. But the residuals are different in the case of the constrained fit as seen in Fig. 4 They are negative at low elevations and increase with increasing elevation, suggesting that the probe is longer (by about 4 µm) along *Z* than along *X* and *Y*.

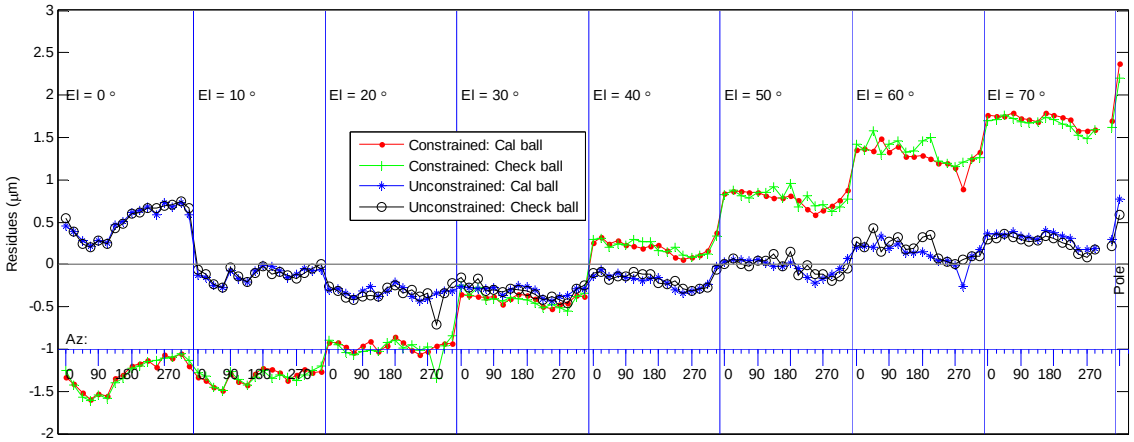

Fig. 4 Residuals from a constrained and unconstrained least-squares best-fit sphere. Data was taken at elevation angles ranging from 0°(the equator) to 70°. At each elevation, 16 points were taken around a circle. In the case of the constrained fit, the center along the Z direction is constrained to the experimentally determined value.

2.3 Ellipsoid fit

We describe the process of fitting an ellipsoid to the measured data in this section. During the calibration process, we estimate nine parameters which include six parameters for the ellipsoid (three radii and three tilt parameters - a, b, c, α, β, χ), and three for the calibration ball (center coordinates - X_O, Y_O, Z_O). The radius of the calibration sphere R is of course a known quantity. During the validation process, we estimate four unknown parameters which are the center of the check sphere (X_O, Y_O, Z_O) and its radius R. We describe the process of fitting an ellipsoid as part of the calibration procedure next.

Calibration

The process of determining the nine unknown parameters from the measured data involves solving a nested non-linear problem with the outer loop formulated as a non-linear least squares problem and the inner loop formulated as a simultaneous system of non-linear equations. Fig. 5(a) shows a schematic of the calibration process. Note that the probe ball, in addition to being ellipsoidal, may also be tilted.

During each iteration of the outer loop, we center the ellipsoid on each of the measured data points and compute the shortest distance between the ellipsoid and the sphere. This collection of shortest distances, the residuals, are determined by solving a simultaneous set of non-linear equations as described next. These residuals are then used to refine the estimates of the nine unknown parameters using a nonlinear least squares minimization method such as the Levenberg-Marquardt or the Gauss-Newton algorithm [5,6].

The purpose of the inner loop, as mentioned earlier, is to determine the shortest distance between the ellipsoid and the sphere when the ellipsoid is centered on any given data point. The current estimates of the nine parameters (assumed to be X_O, Y_O, Z_O, a, b, c, α, β, χ) are used in this calculation.

The data is first translated so that the current estimate for the center of the calibration sphere is the origin. The data is subsequently rotated by the current estimates of the tilt angles so that the polar radius of the probe ball is along the Z axis. Then, let the center of the ellipsoid be at (X_C, Y_C, Z_C), which is the i^{th} measured data point (which has now been translated and rotated as described above). The locus of measured points is shown by the grey line in the figure (before rotation in Fig. 5(a) and after rotation in Fig. 5(b)).

The objective then is to determine the shortest distance between the ellipsoid and the sphere. Let the point on the ellipsoid closest to the sphere be (X_B, Y_B, Z_B) shown as point B in Fig. 5(b), and let the distance between this point and the sphere be t (t is the shortest distance between the sphere and the ellipsoid). Then,

$$\frac{(X_B - X_C)^2}{a^2} + \frac{(Y_B - Y_C)^2}{b^2} + \frac{(Z_B - Z_C)^2}{c^2} = 1 \tag{1}$$

The gradient at B is given by

$$\nabla = 2\left[\frac{(X_B - X_C)}{a^2}\hat{i} + \frac{(Y_B - Y_C)}{b^2}\hat{j} + \frac{(Z_B - Z_C)}{c^2}\hat{k}\right] \tag{2}$$

where $(\hat{i}, \hat{j}, \hat{k})$ are the unit vectors along X, Y, and Z directions. The gradient is normal to the surface of the probe. When the probe is in contact with the sphere, it is also normal to the surface of the sphere, along the radius (direction of OA in Fig. 5). Knowing this direction allows us to project out the components of (R+t) along the three axes. Then, the following three equations can be obtained from the geometry in

Fig. 5(b).

$$\frac{(R+t)(X_B - X_C)}{a^2|\nabla|} + X_B = 0 \tag{3}$$

$$\frac{(R+t)(Y_B - Y_C)}{b^2|\nabla|} + Y_B = 0 \tag{4}$$

$$\frac{(R+t)(Z_B - Z_C)}{c^2|\nabla|} + Z_B = 0 \tag{5}$$

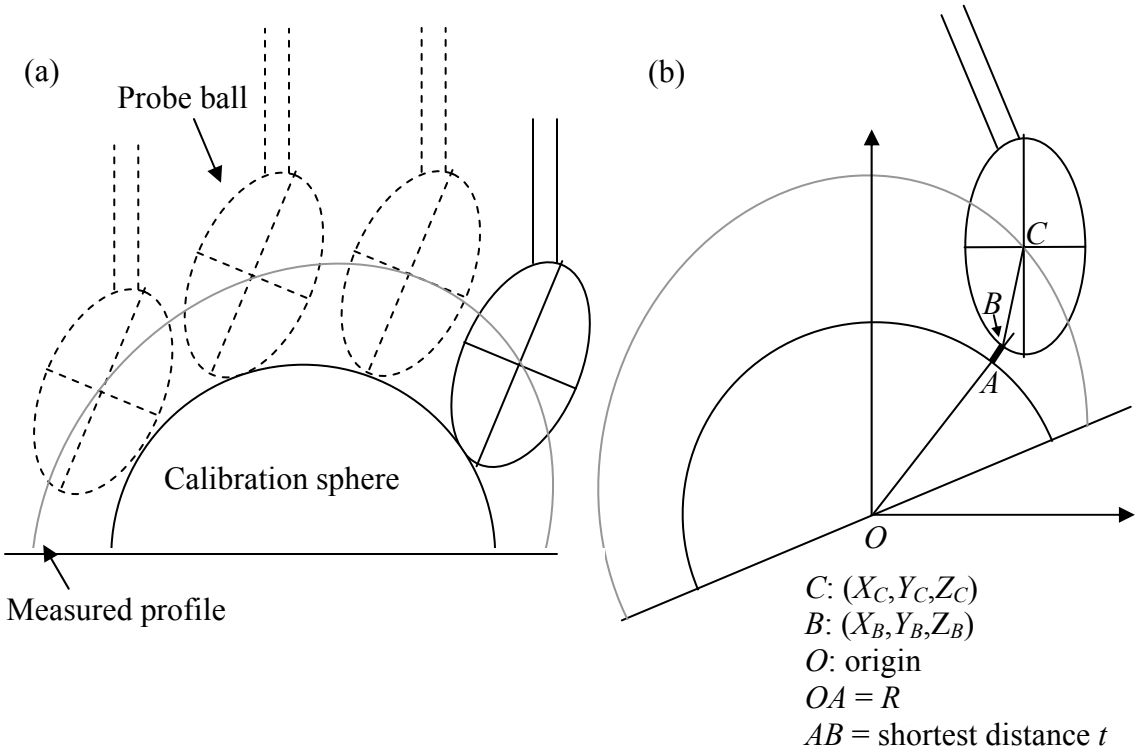

Fig. 5(a) Measurement of a calibration sphere with a tilted ellipsoidal probe. (b) Finding the shortest distance by first translating the center of the sphere to the origin and subsequently rotating the data so that the ellipsoid is vertical.

Eq. 1, 3, 4, and 5 form a system of four nonlinear equations in four unknowns that can be solved using any of the several known iterative techniques [7] to determine both the shortest distance and the coordinate of the point on the ellipsoid closest to the sphere.

Validation

The unknown parameters in the validation process are the center of the sphere (X_O, Y_O, Z_O) and its radius R. The six parameters of the ellipsoid (a, b, c, α, β, χ) are already known. The data is translated so that the current estimate of the center of the sphere is the origin. The data is subsequently rotated so that the ellipsoid is vertical. The inner loop

involves solving Eqs. 1, 3, 4, and 5 to determine the shortest distance between the sphere and the ellipsoid. These residuals are then used to refine the estimates of the unknown parameters using a nonlinear least squares minimization method [5,6].

2.4 Results from calibration and validation measurements

The calibration process indicated that the probe was indeed ellipsoidal. The equatorial radii *a*, *b* were 32.73 µm and 32.58 µm respectively, while the polar radius *c* was 36.18 µm. The ellipsoid was also tilted by a small amount with the three tilt angles α, β, χ being 3.9º, -0.2º, and 12.9º respectively. Note that χ is simply a rotation about the *Z* axis. The diameter of the validation sphere was determined to be 7937.89 µm from the ellipsoid fit. This value is only 10 nm larger than the calibrated diameter of the sphere.

The residuals from the best-fit ellipsoid are shown for both the calibration and the check sphere in Fig. 6. The residuals are within ±0.2 µm for the two spheres at most measurement locations and they agree fairly well from sphere to sphere. In a few instances though, the residuals from sphere to sphere are different by as much as 0.2 µm. This could possibly be due to dirt on the surface. It is also possible that the point of contact on the probe for the two spheres is not identical; this could possibly explain the observed discrepancy in the form from sphere to sphere if the probe ball suffered from large form changes over short distances.

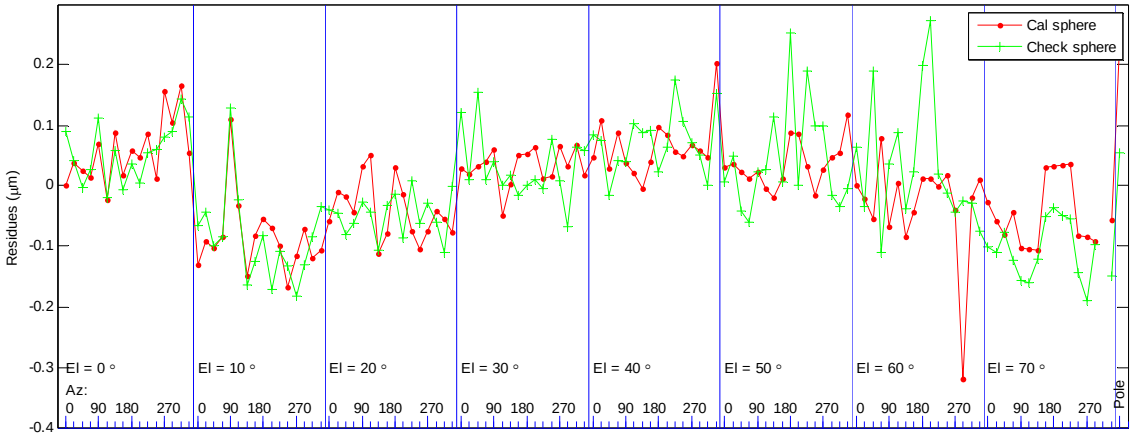

Fig. 6 Residuals from a best-fit ellipsoid for the calibration and check spheres.

As an interesting aside, in Fig. 7 we show experimental confirmation of the claim made in Section 1 about flexible fibers being free to oscillate leading to points of contact that are not the intended point of contact. Fig. 7(a) shows data obtained on the equatorial plane of the 3/16 in sphere over several runs. Fig. 7(b) shows the spread in the data at one azimuthal position alone. It can be seen that the fiber makes contact over a fairly large region along the circumference spanning 12 µm along *X* and 6 µm along *Y*.

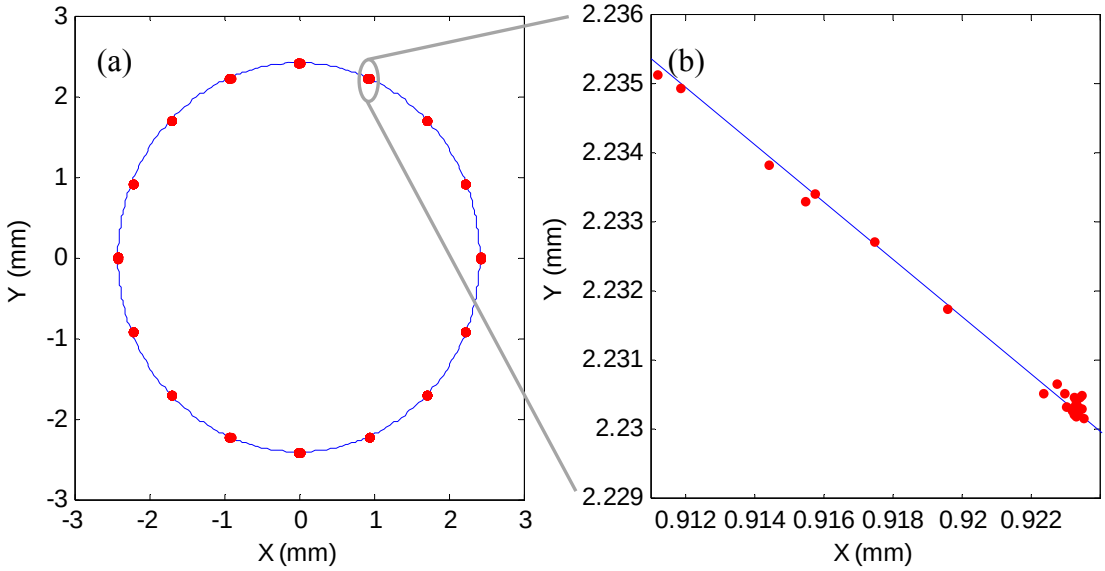

Fig. 7(a) Several runs of data on the equatorial plane of the 3/16 in (4.7625 mm) *sphere. (b) Spread in the data at one azimuthal position alone.*

2.5 Uncertainty considerations

We have performed some Monte Carlo simulations (MCS) that provide an estimate of the uncertainty in the probe parameters and also the uncertainty in the diameter of the check sphere determined using the ellipsoid fit method.

Assuming the standard uncertainty in determining a coordinate in space is 50 nm (somewhat larger than the described in [1] due to small changes in the optical setup and reduced averaging) for the calibration sphere, MCS yields a standard uncertainty of 14 nm for the equatorial radii a and b, 62 nm for the polar radius c, 0.29º for the tilt angles α and β, and 1.29º for the tilt angle χ. These uncertainties in combination with the 50 nm standard uncertainty in determining a coordinate of the check sphere, in turn, translate into a standard uncertainty of 32 nm in the diameter of the check sphere. Considering other sources of uncertainty described in [1], we estimate the combined standard uncertainty in diameter of the check sphere to be 35 nm ($k = 1$).

It should be noted that the probe is free to oscillate due to air currents, and therefore the point of contact on the probe ball for the two spheres may be considerably different from the intended position. If the probe ball form suffers large deviations over short regions on its surface, this will contribute substantially to the uncertainty. We have not developed a comprehensive uncertainty budget yet, but it appears that diameter measurements with an expanded uncertainty of 100 nm ($k = 2$) is feasible with ellipsoidal probes.

3 Three dimensional measurements on a test artifact

3.1 Description

In this section, we describe measurements performed on a conical artifact with our ellipsoidal probe. The artifact has a rounded tip with a nominal 38 μm radius. The half angle of the cone is nominally 20º. We performed circular traces at 12 heights, with 16 sampling points per trace, as shown in Fig. 8. The circular traces from Z = -89 μm to Z = 11 μm are on the conical section of the part, while the remaining six traces are on the hemisphere. We also measured the pole point for a total of 193 data points. The origin of the measured data is set as the center of the hemisphere.

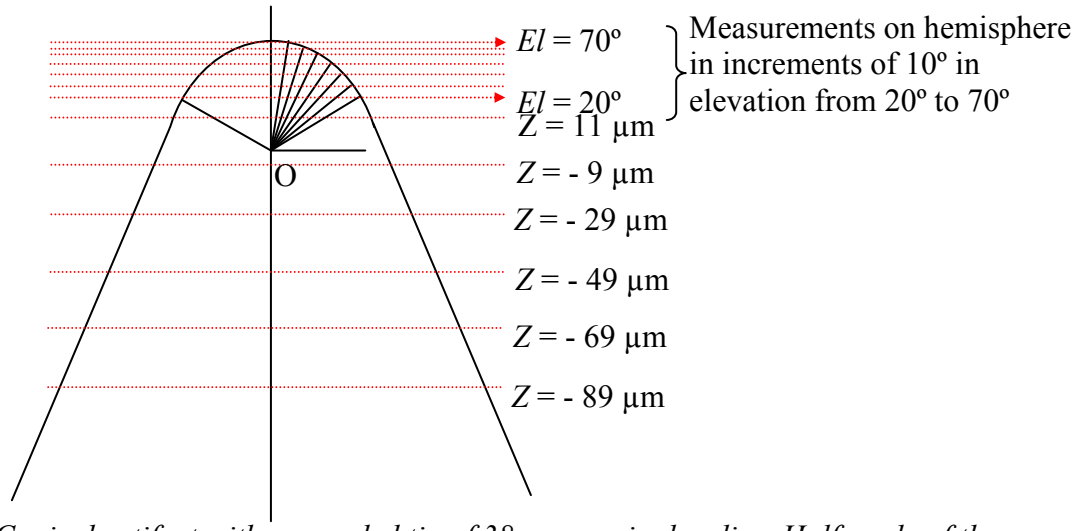

Fig. 8 Conical artifact with a rounded tip of 38 μm nominal radius. Half angle of the cone is nominally 20º.

3.2 Cone-hemisphere fit

From the measured data, we attempt to determine the following seven unknown parameters of the cone-hemisphere geometry: the tilt angles of the cone α, β about the X and Y axes respectively, the half angle θ of the cone, and the center (Xo, Yo, Zo) and radius R of the hemisphere.

Note that a cone in space is defined by six parameters which include: three parameters to define the coordinate of the apex, one parameter for the half angle of the cone, and two parameters for the direction cosines of the axis (the third direction cosine can be determined from the other two because the sum of the squared values of the directions cosines is unity). The additional parameter required to define the hemisphere is its radius. Because it is tangential to the cone, the radius automatically places the center of the hemisphere at a fixed point along the axis.

As described before, we structure the problem in a nested nonlinear manner with the outer loop formulated as a nonlinear least squares problem and the inner loop as a set of four nonlinear equations in four unknowns. For each iteration of the outer loop, we determine the residue (the shortest distance between the probe and the cone-hemisphere artifact) for each measured data point. These residuals are then used to refine the current

estimates of the seven unknown parameters using non-linear least squares minimization techniques such as the Levenberg-Marquardt algorithm.

In order to determine the residuals, we have to determine the shortest distance between the probe and the cone-hemisphere artifact. If the measured data belongs to the hemispherical tip, the residuals can be determined as described in Section 2.3. If the measured data belongs to the conical surface, a separate procedure is required which is described in this section.

The three tilt and three radii parameters of the ellipsoid are already known from the calibration on a master sphere, see Section 2.3. To determine the shortest distance between an ellipsoid and the cone, we require the current estimates of the seven unknown parameters of the cone-hemisphere geometry; let these be Xo, Yo, Zo, R, α, β, and θ. Fig. 9(a) shows the probe centered on the i^{th} measured data point, given by C. In Fig. 9(a), the probe is shown to be oriented along the vertical direction; because the probe tilt parameters are a known quantity, the entire data is first rotated so the probe is vertically oriented.

Given the probe is centered on measured data point C (X_C, Y_C, Z_C), the objective then is to determine the coordinate (X_B, Y_B, Z_B) of the point B that is closest to the cone and the shortest distance t given by AB in Fig. 9(a). We formulate the problem as a system of four nonlinear equations in four unknowns that can be solved using known iterative techniques [7].

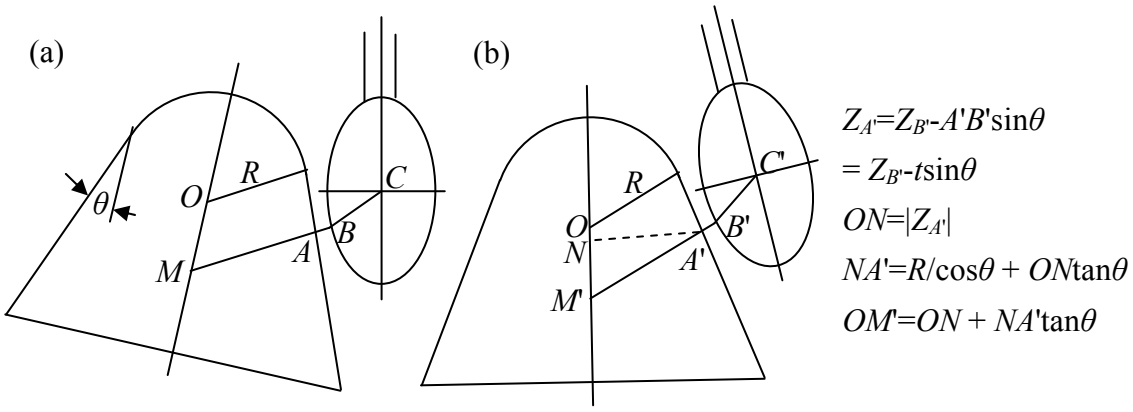

Fig. 9(a) Determining the shortest distance between the ellipsoid and the tilted con-hemisphere geometry. (b) Rotating the cone-hemisphere geometry so that it is vertical.

The ellipsoid in Fig. 9(a) can be described by

$$\frac{(X_B - X_C)^2}{a^2} + \frac{(Y_B - Y_C)^2}{b^2} + \frac{(Z_B - Z_C)^2}{c^2} = 1 \qquad (6)$$

The gradient at B (which is along the direction of vector BM, perpendicular to the surfaces of the cone and the probe) is given by

$$\nabla = 2\left[\frac{(X_B - X_C)}{a^2}\hat{i} + \frac{(Y_B - Y_C)}{b^2}\hat{j} + \frac{(Z_B - Z_C)}{c^2}\hat{k}\right] \tag{7}$$

The following three equations can be obtained from the geometry in Fig. 9(a)

$$X_M - MB\frac{(X_B - X_C)}{a^2|\nabla|} - X_C = 0 \tag{8}$$

$$Y_M - MB\frac{(Y_B - Y_C)}{b^2|\nabla|} - Y_C = 0 \tag{9}$$

$$Z_M - MB\frac{(Z_B - Z_C)}{c^2|\nabla|} - Z_C = 0 \tag{10}$$

where (X_M,Y_M,Z_M) is the coordinate of M. If the coordinate of M can be expressed in terms of the unknown parameters (X_B, Y_B, Z_B, t), the system of four equations given by Eqs. 6, 8, 9, and 10, can be solved as a simultaneous system of four nonlinear equations in four unknowns. Expressing the coordinate of M in terms of the unknowns can be accomplished fairly easily by some simple coordinate system rotations as described next.

Let the data set be rotated (using current estimates of the tilt angles for the cone-hemisphere artifact) so that the cone-hemisphere artifact is oriented along the vertical direction. Therefore, point C is now represented by C' in the new frame and its coordinate is given by

$$(X_{C'}, Y_{C'}, Z_{C'})^T = Rx^{-1}Ry^{-1}(X_C, Y_C, Z_C)^T \tag{11}$$

where Rx and Ry are the rotation matrices based on current estimates of the tilt angles α and β respectively, and the superscript T refers to the transpose of the array. Note that the coordinate of point C is a known quantity (it is a measured data point). The rotation matrices are also known (from the current estimates for the tilt angles) and therefore the coordinate of C' is a known quantity. The coordinate of the unknown point B is related to the point B' in the rotated frame through the following:

$$(X_{B'}, Y_{B'}, Z_{B'})^T = Rx^{-1}Ry^{-1}(X_B, Y_B, Z_B)^T \tag{12}$$

The distance AB in Fig. 9(a) is the shortest distance t, and is unchanged due to rotation. Therefore $A'B' = AB = t$.

From the geometry in Fig. 9(b), OM' is given by

$$OM' = ON + NA'\tan\theta = \left|Z_{B'} - t\sin\theta\right| + (R/\cos\theta + \left|Z_{B'} - t\sin\theta\right|\tan\theta) \tag{13}$$

The coordinate of point M' in terms of the unknown parameters t and $Z_{B'}$ is therefore $(0,0,-(\left|Z_{B'} - t\sin\theta\right| + (R/\cos\theta + \left|Z_{B'} - t\sin\theta\right|\tan\theta)))$. The coordinate of point M can be

obtained from the coordinate of M' as

$$(X_M, Y_M, Z_M)' = RyRx(X_{M'}, Y_{M'}, Z_{M'}) \tag{14}$$

The distance $M'B'$ is given by

$$M'B' = R + OM' \sin\theta + t \tag{15}$$

Thus, we have expressed the coordinate of M and the distance MB in terms of the unknown parameters (X_B, Y_B, Z_B, t). Eqs. 6, 8, 9, and 10 can therefore be solved to determine the residue t for any given data point C.

3.4 Results

We initially analyzed the cone and hemisphere data independently to assess the form of each portion separately. The residuals of the data collected on the conical surface from a least squares best fit cone are shown in Fig. 10. The cone appears to be three-lobed but the magnitude of the form is not too large (less than 1 μm). The residuals of the data collected on the hemispherical surface from a least squares best fit sphere are shown in Fig. 10 as well. The lobing error is not as pronounced on the hemisphere. There appears to be a large form error, with the trace at 20º being larger than nominal by at least 0.5 μm.

In addition to the form error, our least squares fit indicated that the hemisphere and cone were shifted in space. We estimated this shift as follows. As mentioned earlier, we first determined the center and radius of the hemisphere through least-squares best fit to the data acquired from the hemisphere. Let this radius be r. Then, we fit a least-squares best fit cone to the data acquired on the conical surface. We determined the position along the axis on the cone where a hemisphere of radius r can be centered so that it will be tangent to the cone. For the ideal geometry, this point on the cone will coincide with the center of the hemisphere as determined from its best-fit. In the case of our example, the center of the hemisphere was away from the corresponding point on the cone by about (-2, -0.3, 4.7) μm in (x, y, z) respectively. That is, the hemisphere appeared to be shifted in space from the cone by the amounts indicated.

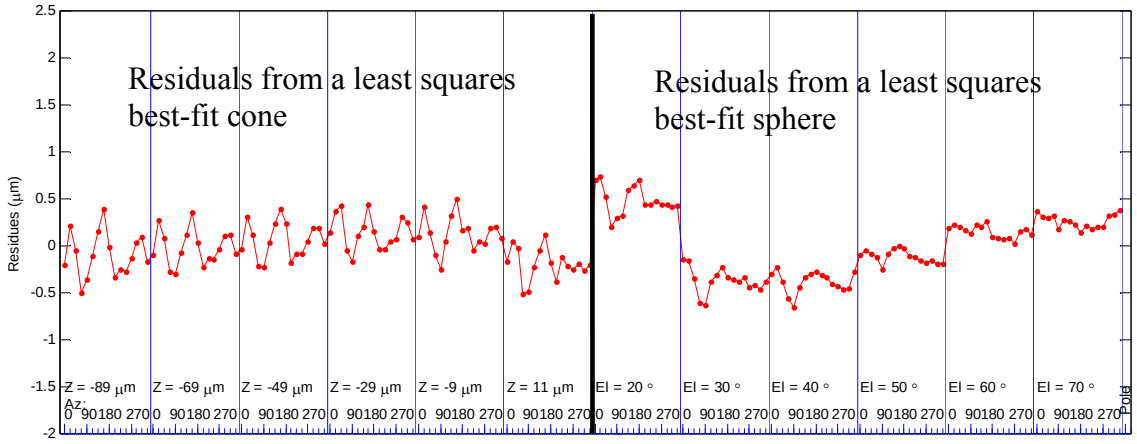

Fig. 10 Residuals from a least squares best fit cone and from a least squares best fit sphere.

We then performed a simultaneous fit of a cone and hemisphere to the data. The residuals from such a fit are shown in Fig. 11. Notice that the residuals are much larger than those in Fig. 10. We suspected the reason for this discrepancy to be from the shift in the centers of the cone and the hemisphere, and a simulation, in fact, confirmed this. The simulation comprised a data set closely mimicking the measured data set and incorporating the shift in the centers between the cone and the hemisphere, and also the form error seen in the hemisphere. The simulation results are shown in Fig. 11. The simultaneous cone-hemisphere least-squares fit and the simulation provide strong evidence that the hemisphere and the cone are in fact shifted in space, thus providing valuable measurement feedback to the manufacturing process.

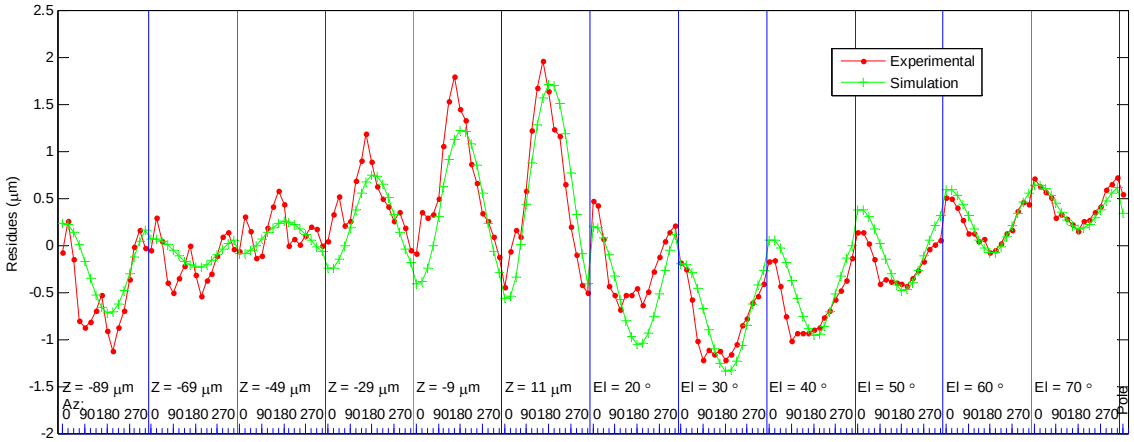

Fig. 11 Simultaneous fitting of a cone and a sphere to the data set. Residuals for both measured and simulated data.

4 Summary

In this paper, we describe some issues pertaining to three dimensional measurements of micro-features using flexible fiber probes that may have a non-spherical tip. Unlike macroscopic probes measuring macro-scale artifacts, the flexible fiber probes are free to oscillate and can therefore contact the part away from the intended position. Because the part sizes are comparable to probe sizes, the direction of the surface normal at the point of contact may be significantly different from the approach direction. In addition, the probe ball itself may be non-spherical. The probes we use for the NIST fiber probe can be better approximated as an ellipsoid than as a sphere. These factors make probe radius compensation a challenging problem. In this paper, we have described a process to calibrate and validate the probe shape and size using least-squares ellipsoid fits to measurements made on master spheres. We also demonstrate how we may perform probe size/shape compensation of the measured data to obtain surface coordinates on micro-scale three dimensional artifacts.

In our experiments with integrally manufactured fiber probe tips, we have noticed that

our probe ball is more closely modeled as an ellipsoid than as a sphere. The equatorial radii of the probe used in the experiments described in this paper were 32.73 μm and 32.58 μm, while the polar radius was 36.18 μm. The form deviations (residuals from an ellipsoid fit) were within ±0.2 μm of the nominal geometry, the ellipsoid. We estimated the diameter of the check sphere, using ellipsoidal fits, to within 10 nm of the calibrated value, thus providing a validation of our methods. Our measurements on microscale features suggest that our approach of least-squares fitting can be used to perform probe size/shape compensation when the probe ball is nominally ellipsoidal. Even when the shape is not ellipsoidal, the method of least-squares may be employed in finding the best-fit geometry of the probe; this information can then be employed during probe size/shape compensation.

Acknowledgements

We gratefully acknowledge the assistance of Roy Sundahl, Mike Braine and Eric Stanfield at NIST. We thank Dr. Vijay Srinivasan for reviewing this paper.

References

1. B. Muralikrishnan, Jack Stone and John Stoup, "Fiber deflection probe for small hole metrology," Precision Engineering, 30 (2), 2006
2. A Weckenmann, G Peggs and J Hoffmann, "Probing systems for dimensional micro- and nano-metrology, Measurement Science and Technology", v17n2, 504-509, 2006
3. A. Weckenmann, T. Estler, G. Peggs and D. McMurtry, "Probing Systems in Dimensional Metrology", CIRP Annals - Manufacturing Technology, Volume 53, Issue 2, 2004, Pages 657-684
4. Probes manufactured by WT&T Inc., Canada.
5. Shakarji, C., "Least-squares fitting algorithms of the NIST Algorithm Testing System," Journal of Research of the NIST, 103 (6), pp. 633-641, 1998.
6. Forbes, A.B., Least-Squares Best-fit Geometric Elements, NPL Report DITC 140/89, National Physical Laboratory, Great Britain, 1989.
7. William H. Press, Brian P. Flannery, Saul A. Teukolsky, William T. Vetterling, Numerical Recipes in C: The Art of Scientific Computing, Cambridge University Press; 2 edition (October 30, 1992)